Cement and Concrete Research 90 (2016) 127–136

Contents lists available at ScienceDirect

Cement and Concrete Research

journal homepage: www.elsevier.com/locate/cemconres

# Fatigue-induced deterioration of the interface between micro-polyvinyl alcohol (PVA) fiber and cement matrix

Jishen Qiu, Xin-Ni Lim, En-Hua Yang *

*School of Civil and Environmental Engineering, Nanyang Technological University, Singapore 639798*

ARTICLE INFO

*Article history:*
Received 20 January 2016
Received in revised form 12 July 2016
Accepted 9 August 2016
Available online xxxx

*Keywords:*
Fatigue
Fiber-matrix interface
Fiber-reinforced cementitious composites
FRC
Single fiber pullout

ABSTRACT

Quality of interfacial bond between fibers and matrix determines the post-cracking behavior of fiber-reinforced composites. Fatigue-induced interface deterioration between fibers and matrix has not been investigated systematically which prevents understanding of premature failure of fiber-reinforced composites subject to fatigue. This study experimentally investigated the deterioration mechanism of flexible fibers in brittle matrix subject to fatigue load. Specifically, the effect of fatigue-induced deterioration of interface between micro-PVA fiber and cement matrix was studied through the single fiber fatigue pullout tests and the micro-structural deterioration mechanism of the fiber-matrix interface under fatigue load was unveiled. It was found that fatigue load leads to fiber debonding which can be described by an empirical relation similar to the Paris' law. Fatigue-induced interface hardening can occur during fiber debonding stage as well as fiber slippage stage. Oil-treatment on surface of micro-PVA fiber was demonstrated as a mean to mitigate such fatigue-induced interface hardening.



## 1. Introduction

High strength and/or high stiffness engineered composites, including polymers, metallic composites, ceramics, and cement-based concrete, are widely used in manufacturing and construction industry. As a result of the enhanced strength and stiffness, they suffer from severe brittleness and are prone to fracture. Micro-fibers, either long continuous or short dispersed, are added into matrix to improve the cracking resistance and to increase the fracture toughness of engineered composites [1–4].

Fiber-reinforced cement-based composites (FRCC) represent a special group of fiber-reinforced engineered composites. Compared with aforementioned composites, it is used in a much greater volume to manufacture large-scale components for buildings and infrastructures [5]. For the ease of processing and on-site casting, most FRCC adopt dispersed short fibers instead of aligned continuous fibers. FRCC technology has been developing for almost 50 years. Various types of fibers, including natural fibers [6], carbon fibers [7], metallic fibers [8], and polymeric fibers [9,10], have been adopted for enhancing the fracture toughness, improving material durability [11,12], and even designing new attributes into FRCC. Under fire, for instance, the relatively low melting point of polypropylene (PP) fibers is taken advantage of to release the heat-induced internal vapor pressure and prevent matrix spalling [13]. The high electrical conductivity of carbon fibers is used for creating self-sensing concrete for damage detection [14].

In FRCC, matrix crack propagation is controlled by the post-cracking fiber-bridging, which is fundamentally governed by the fiber-matrix interfacial bond as well as the fiber strength. By the nature of interfacial bond and fiber strength, the fibers used in FRCC can be categorized into two groups: the stiff metallic and carbon fibers, with relatively higher strength and weaker bond to cement matrix, are usually completely pulled out from the matrix during fiber-bridging failure [15,16]. On the contrary, the flexible natural and polymeric fibers, with relatively lower strength and stronger bond to cement matrix, could be ruptured before they are pulled out [17,18]. Compared with the stiff fibers, the fiber-bridging failure of flexible fiber-reinforced system is more complicated as it involves fiber pullout as well as fiber rupture.

In many applications, such as pavement, bridge deck, railway slippers, and the supporting structure of offshore windmills, FRCC are subject to fatigue from repeated loads. Herein the fatigue performance of FRCC, especially the fiber-bridging deterioration under repeated loading, is of great importance. The fatigue performance of FRCC, both the stiff fiber-reinforced system [19–21] and the flexible fiber-reinforced system [21–26], have been studied extensively. Compared with normal concrete, the fatigue life of FRC is greatly extended. However, it was observed that FRCC may experience premature failure under fatigue loading. For instance, Jun and Mechtcherine [22,23] compared the PVA fiber-reinforced strain-hardening cement-based composites (SHCC) failed by low-cycle cyclic loading to the control group failed by monotonic loading, and found that the crack number was slightly reduced while the crack width was enlarged. Muller et al. [24] studied PVA fiber-reinforced SHCC performance under strain-controlled high-cycle fatigue loading

* Corresponding author at: N1-01b-56, 50 Nanyang Avenue, 639798, Singapore.
*E-mail address:* ehyang@ntu.edu.sg (E.-H. Yang).

http://dx.doi.org/10.1016/j.cemconres.2016.08.021
0008-8846/

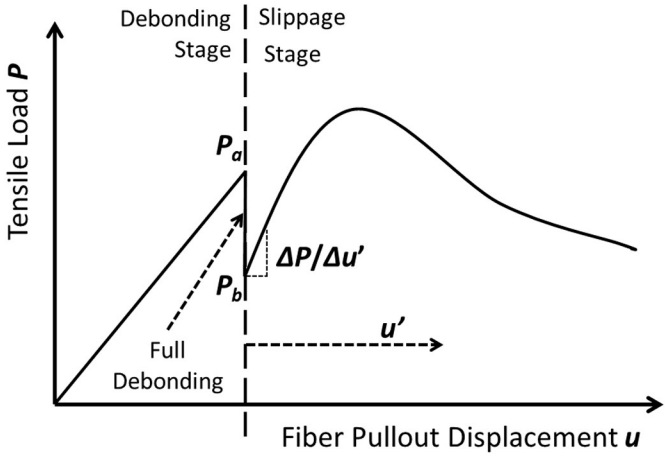


**Fig. 1.** Typical single fiber pullout load vs. pullout displacement u relation from single micro-PVA fiber monotonic pullout test.

and found the tensile ultimate strain decreased with decreasing strain increment and increasing load cycles. Qian [25] and Suthiwarapirak et al. [26] studied performance of PVA fiber-reinforced engineered cementitious composite (ECC) under load-controlled high-cycle fatigue loading and also found that the crack number decreased with increasing load cycles. The morphology of the fracture surface in [26] suggested that the fiber-bridging behavior must have been altered under fatigue, as the ratio of ruptured to pulled-out fibers was remarkably increased with load cycles.

Fundamentally, such fatigue-dependency of fiber-bridging in FRCC can be attributed to the fatigue-induced deterioration of fiber and fiber-cement interface. While the fatigue-induced flexible fiber strength deterioration in cement matrix was investigated [27], the possible deterioration of interfacial bond between the flexible fiber and hard cement matrix under fatigue load was rarely studied. It represents a knowledge gap which prevents FRCC from being tailored for improvement on fatigue performance. This study experimentally investigated the deterioration mechanism of flexible fibers in cement matrix subject to fatigue load. Specifically, the effect of fatigue-induced deterioration of interface between micro-PVA fiber and cement matrix was studied; the microstructural deterioration mechanism of the fiber-matrix interface under fatigue loading was unveiled. The insight obtained from this study help to improve FRCC fatigue performance; more importantly the methodology can be extended to analyze and tailor other flexible fiber-reinforced brittle-matrix composites.

## 2. Experimental program

Single fiber pullout test suggested by Redon et al. [18] has been widely used to study the micro-fiber/matrix interface properties,

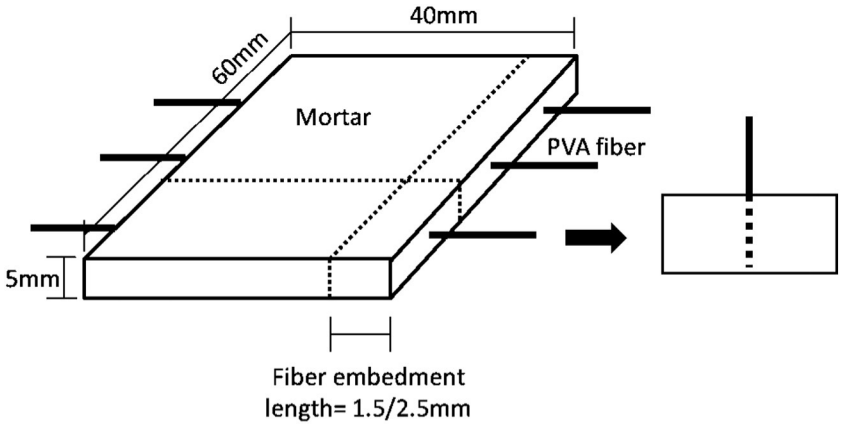


(a)

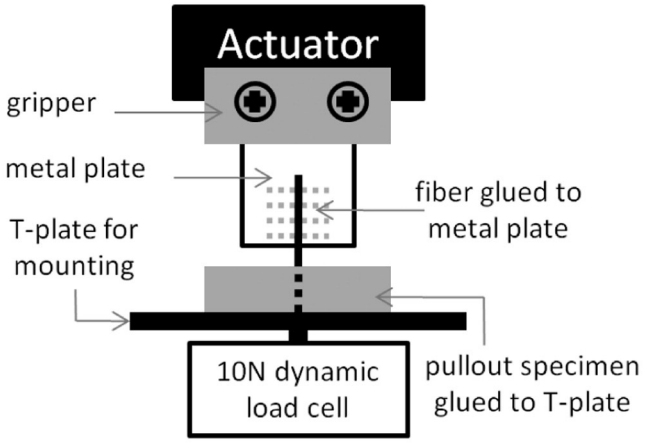


(b)

**Fig. 2.** Experimental set up: (a) preparation of the single fiber pullout specimen; and (b) illustration of the specimen assembled to the mechanical testing system.

which can be derived from the fiber pullout load versus fiber end displacement curve as shown in Fig. 1. Current study adopted similar setup as shown in Fig. 2 except that the loading scheme was different. Displacement-controlled pullout was often used in the single fiber monotonic pullout test. In this study, load-controlled cyclic load was used in the single fiber fatigue pullout test. Detailed loading scheme will be introduced in the following section. The fatigue load was introduced by an MTS Acumen™ 1 Electrodynamic Test System, which was specially developed for the dynamic tests with low loading levels. This testing system has a dynamic capability of ±10 mm displacement at 10 Hz with a maximum load of 1080 N. A 10 N dynamic load cell was included in the system for closed-loop loading control at the low loading level in current test.

### 2.1. Specimen preparation

Micro-polyvinyl alcohol (PVA) fiber was used in current study as a typical flexible fiber. Polyvinyl alcohol is hydrophilic due to the existence of hydroxyl function group. As a result, the bond between PVA fiber and surrounding matrix can be very strong, which may cause premature fiber rupture during pullout. Surface treatment by coating oil to PVA fibers is often adopted as a technique to reduce the interfacial bond and to mitigate the fiber rupture [28]. In this study, therefore, PVA fibers both with and without surface oil-treatment was investigated. The properties of the non-oil-coated (NOC) and oil-coated (OC) PVA fiber are given in Table 1.

The cement-based mortar matrix, in which the PVA fiber was embedded, was made of type I Portland cement (CEM I 52.5), ground granulated blast-furnace slag (GGBS), and sieved river sands (<0.6 mm in particle size), superplasticizer, and water. The mix design of the mortar is given in Table 2, the water to binder ratio was set as 0.30. The 28-day compressive strength of the mortar matrix was 70.8 ± 1.8 MPa.

The specimen preparation follows the suggestions of reference [29]. A long PVA fiber was cut into about 150 mm in length and embedded into the fresh mortar as shown in Fig. 2a. The hardened specimen was demolded after one day and cut into thin specimens (1.5 mm in thickness) with a single fiber extruded out from one side. The relatively small embedment length assured that the fiber was pulled out instead of being ruptured during the test. A thicker specimen of 2.5 mm was used to study the fatigue-induced debonding of oil-coated fiber because a reduced interfacial bond was expected for the oil-coated fiber.

### 2.2. Single fiber fatigue pullout test

The single fiber fatigue pullout test consisted of a load-controlled fatigue preloading followed by a displacement-controlled monotonic pullout reloading. The fatigue preloading was meant to introduce interface deterioration at different loading levels and fatigue cycles and the monotonic reloading was used to determine the fiber-matrix interface properties after the fatigue, and thereby the fatigue-induced deterioration of interface between the fiber and the matrix can be quantified. The load-controlled tensile fatigue preloading consisted of a ramping phase and a cyclic phase as illustrated in Fig. 3. Table 3 summarizes the experimental program and loading scheme. Single fiber pullout specimen subject to monotonic pullout was also tested as the control.

**Table 1**
Properties of micro-PVA fibers.

| Fiber surface treatment | Nominal diameter (μm) | Young's modulus (GPa) | Density (kg/m$^3$) | Surface oil coating by mass (%) |
|---|---|---|---|---|
| Non-oil-coated (NOC) | 41.8 | 41 | 1300 | 0.0 |
| Oil-coated (OC) | 44.7 | 41 | 1300 | 1.2 |

**Table 2**
Mix proportions of mortar matrix.

| Cement (kg/m$^3$) | GGBS (kg/m$^3$) | Sand (kg/m$^3$) | Water (kg/m$^3$) | Superplasticizer (kg/m$^3$) |
|---|---|---|---|---|
| 551 | 827 | 276 | 414 | 2.4 |

Typical single fiber pullout curve subject to monotonic loading is illustrated in Fig. 1. During the fiber debonding stage, fiber pullout force increases with fiber end displacement accompanied with tunnel crack propagation along the fiber-matrix interface until the fiber was fully debonded from matrix. A sudden load drop from $P_a$ to $P_b$ indicates completion of debonding followed by slippage stage with large displacement. The fiber-matrix interface properties, including chemical bond $G_d$, frictional bond $\tau_0$, and slip-hardening coefficient $\beta$, can be derived from the single fiber pullout curve accordingly [18].

$$G_d = \frac{2(P_a - P_b)^2}{\pi^2 E_f d_f^3} \tag{1}$$

$$\tau_0 = \frac{P_b}{\pi d_f L_e} \tag{2}$$

$$\beta = \frac{d_f}{L_e} \cdot \left( \frac{\Delta P / \Delta u'|_{u' \to 0}}{\tau_0 \pi d_f} + 1 \right) \tag{3}$$

where $E_f$ is the Young's modulus of fiber; $d_f$ is the fiber diameter; $L_e$ is the fiber embedment length; $\Delta P/\Delta u'$ is the initial slope of the $P$ versus $u'$ curve where $u'$ approaches 0 as in Fig. 1.

For the single fiber fatigue pullout test, three fatigue loading levels, i.e. $P_{max} << P_a$, $P_{max} < P_a$, and $P_{max} > P_a$, and a wide range of fatigue cycles up to 500,000 cycles were tested in this study to introduce different levels of fatigue-induced interface deterioration. At relatively low fatigue loading level ($P_{max}$ ~ 0.3 to 0.4 N ≪ $P_a$), fiber were unlikely to experience full debonding even at the end of the fatigue cycles. The results therefore were used to understand the fatigue-induced deterioration in the fiber debonding stage. At the medium fatigue loading level ($P_{max}$ ~ 0.4 to 0.5 N < $P_a$), the full debonding might occur during the fatigue cycles, and the results were used to determine the fatigue-induced fiber debonding rate, i.e. the tunnel crack propagation rate. At relatively high fatigue loading level ($P_{max}$ ~ 0.5 to 0.7 N > $P_a$), the $P_{max}$ was likely to exceed the debonding force $P_a$, and the fiber

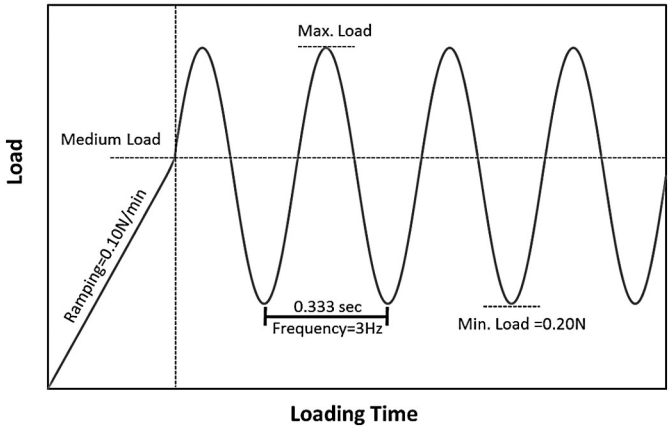


**Fig. 3.** Loading scheme of the fatigue preloading.

**Table 3**
Summary of experimental program and loading scheme.

| Fiber type | Loading type | Embedment length, $L_e$ (mm) | Testing procedure | | |
|---|---|---|---|---|---|
| | | | Fatigue preloading (load-control) | | Monotonic reloading (displacement-control) |
| | | | $P_{max}$ (N) | Load cycles (thousands) | |
| NOC fibers | Monotonic (control) | 1.5 | N.A. | | 0.03 mm/min |
| | Low level fatigue | 1.5 | 0.35–0.40 | 10–500 | |
| | Medium level fatigue | 1.5 | 0.40–0.50 | 10–500 | |
| | High level fatigue | 1.5 | 0.50–0.70 | 1–100 | |
| OC fibers | Monotonic (control) | 1.5 | N.A. | | |
| | Low level fatigue | 2.5 | 0.30–0.40 | 5–20 | |
| | High level fatigue | 1.5 | 0.60–0.70 | 1–10 | |

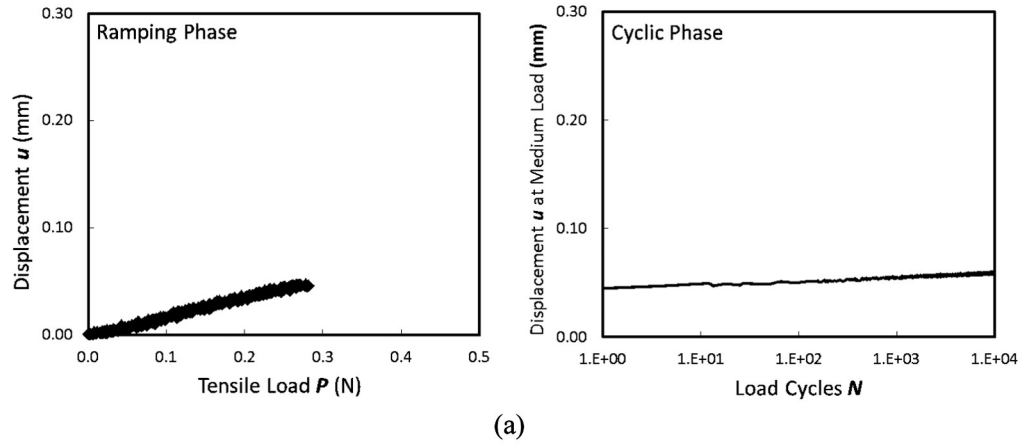


**Fig. 4.** Displacement history of single fiber pullout specimen subject to (a) low, $P_{max} = 0.35\ \text{N} << P_a$; (b) medium, $P_{max} = 0.5\ \text{N} < P_a$; and (c) high, $P_{max} = 0.70\ \text{N} > P_a$, fatigue loading levels.

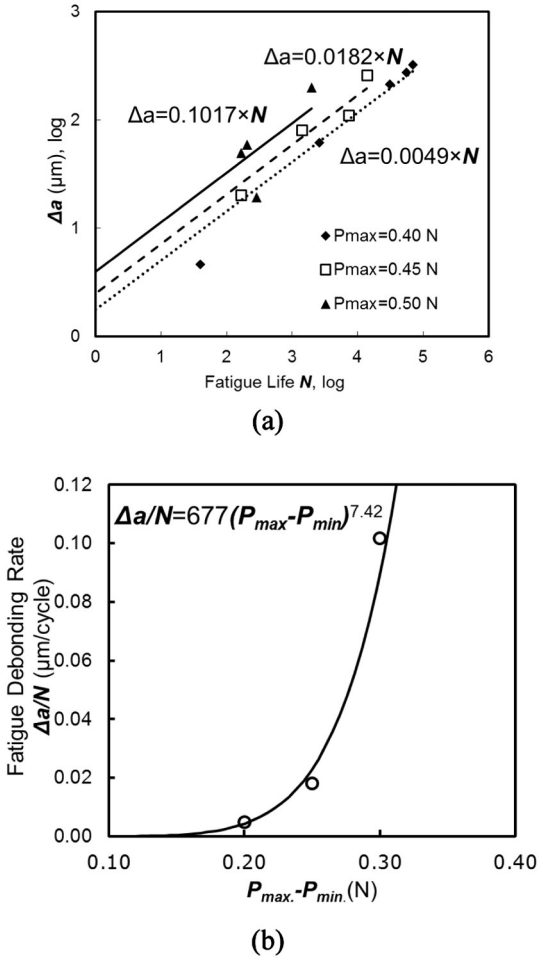


**Fig. 5.** (a) Tunnel crack propagation $\Delta a$ along the fiber-matrix interface as a function of fatigue cycles and fatigue loading levels, both Y- and X-axes are draw in logarithmic for illustration; and (b) fatigue-induced fiber debonding rate ($\Delta a/N$) as a function of fatigue load ($P_{max} - P_{min}$).

fully debonded from the matrix during the fatigue ramping stage. The results therefore were used to understand the fatigue-induced deterioration in the fiber slippage stage.

## 3. Results and discussion

Section 3.1 reports the results of single fiber fatigue pullout test on non-oil-coated (NOC) fibers to characterize the fatigue-induced fiber-matrix interface deterioration. Test results on OC fibers reported in section 3.2 evaluates the effect of fiber surface treatment on the interface deterioration under fatigue load.

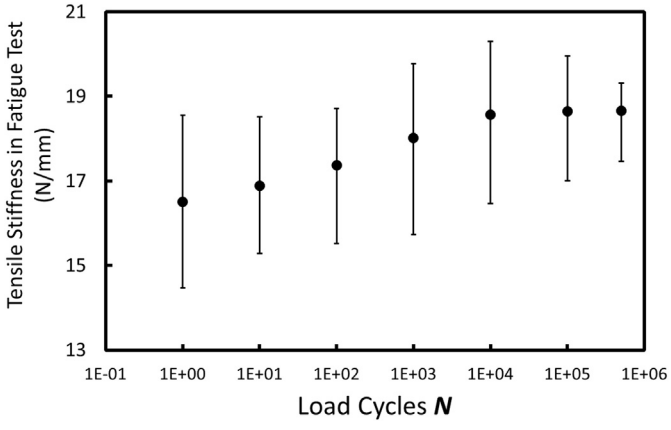


**Fig. 6.** Change of tensile stiffness in the cyclic phase of the fatigue test ($P_{max} = 0.35$ N).

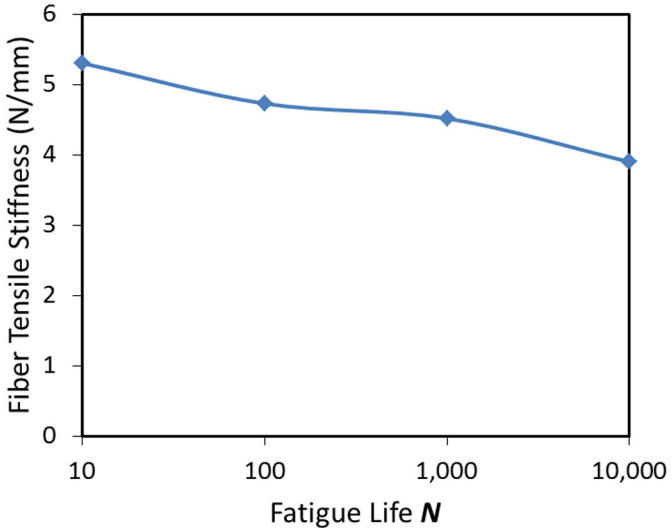


**Fig. 7.** Fiber stiffness as a function of fatigue cycle.

### 3.1. Fatigue-induced fiber-matrix interface deterioration

Fig. 4 shows the displacement history as a function of applied load in the ramping phase and as a function of fatigue cycles in the cyclic phase at the three fatigue loading levels (low, medium, and high). At relatively low fatigue loading level, fiber displacement increases linearly with applied load in the ramping phase. After that, fiber displacement increases slowly with fatigue cycles (Fig. 4a) indicating slow degradation of the fiber-matrix interface, which is likely due to debonding of the fiber from the matrix under fatigue. This suggests the fatigue-induced tunnel crack propagation was very slow and fiber displacement was very limited at relatively low fatigue loading level, and the full-debonding did not take place even at the end of the fatigue test. This was used to study the effect of fatigue on fiber-matrix interface before full debonding where limited fiber displacement was expected.

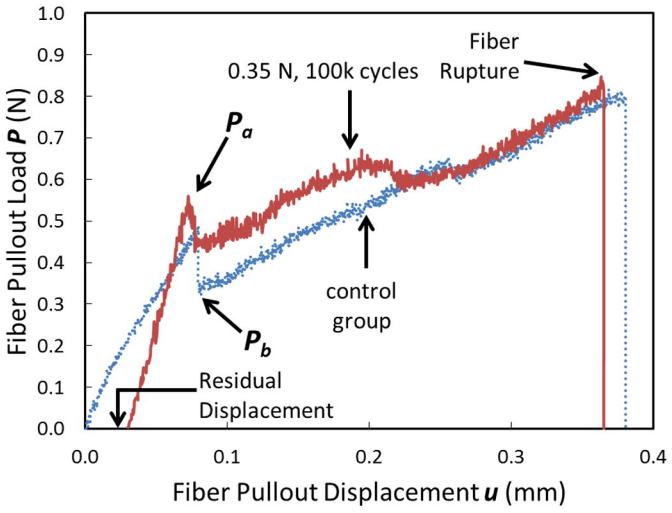


**Fig. 8.** Typical fiber pullout load-displacement ($P$-$u$) relation of control specimen and specimen that has experienced relatively low-level fatigue load ($P_{max} \leq 0.40$ N).

At the medium fatigue loading level (Fig. 4b), sudden displacement leap was observed during fatigue cycling. In the displacement-controlled single fiber monotonic pullout test, the event of complete debonding was noticed with a sudden load drop as shown in Fig. 1. In the load-controlled single fiber fatigue pullout test; however, full debonding should be accompanied with a sudden displacement leap as shown in Fig. 4b. Current study demonstrates that fatigue loads are indeed able to initiate tunnel crack propagation and eventually cause complete debonding of fiber from the surrounding matrix. Such fatigue-induced fiber debonding was observed and reported for the first time. This can be used to quantitatively determine the fatigue-induced fiber debonding rate.

At relatively high fatigue loading level (Fig. 4c), sudden displacement leap occurred during the ramping phase, which indicates the full debonding of the fiber from the matrix happened even before the first cycle of fatigue load. This implies fiber experienced relatively large slippage during fatigue cycles. This was then used to study the effect of fatigue on fiber-matrix interface after full debonding where relatively large fiber displacement results.

*3.1.1. Fatigue-induced fiber debonding*

As shown in Fig. 4b, a sudden displacement leap in the load-controlled single fiber fatigue pullout test indicates complete debonding of fiber during the fatigue test. To quantify fatigue-induced fiber debonding rate, three medium fatigue loading levels (0.40 N, 0.45 N, and 0.50 N) were tested. Fig. 5a plots the relation between fatigue-induced tunnel crack propagation length $\Delta a$ along fiber-matrix interface and number of cycles $N$ to full debonding under the three medium fatigue loading levels. $\Delta a$ was calculated based on the Eq. (4).

$$\Delta a = L_e - a_0 \tag{4}$$

where $L_e$ is the fiber embedment length, and $a_0$ is the debonding length at the end of the ramping phase (Fig. 3), which can be determined through Eq. (5).

$$a_0 = \frac{P_{max} - \sqrt{\pi^2 G_d E_f (1+\eta) d_f^3 / 2}}{\pi \tau_0 (1+\eta) d_f} \tag{5}$$

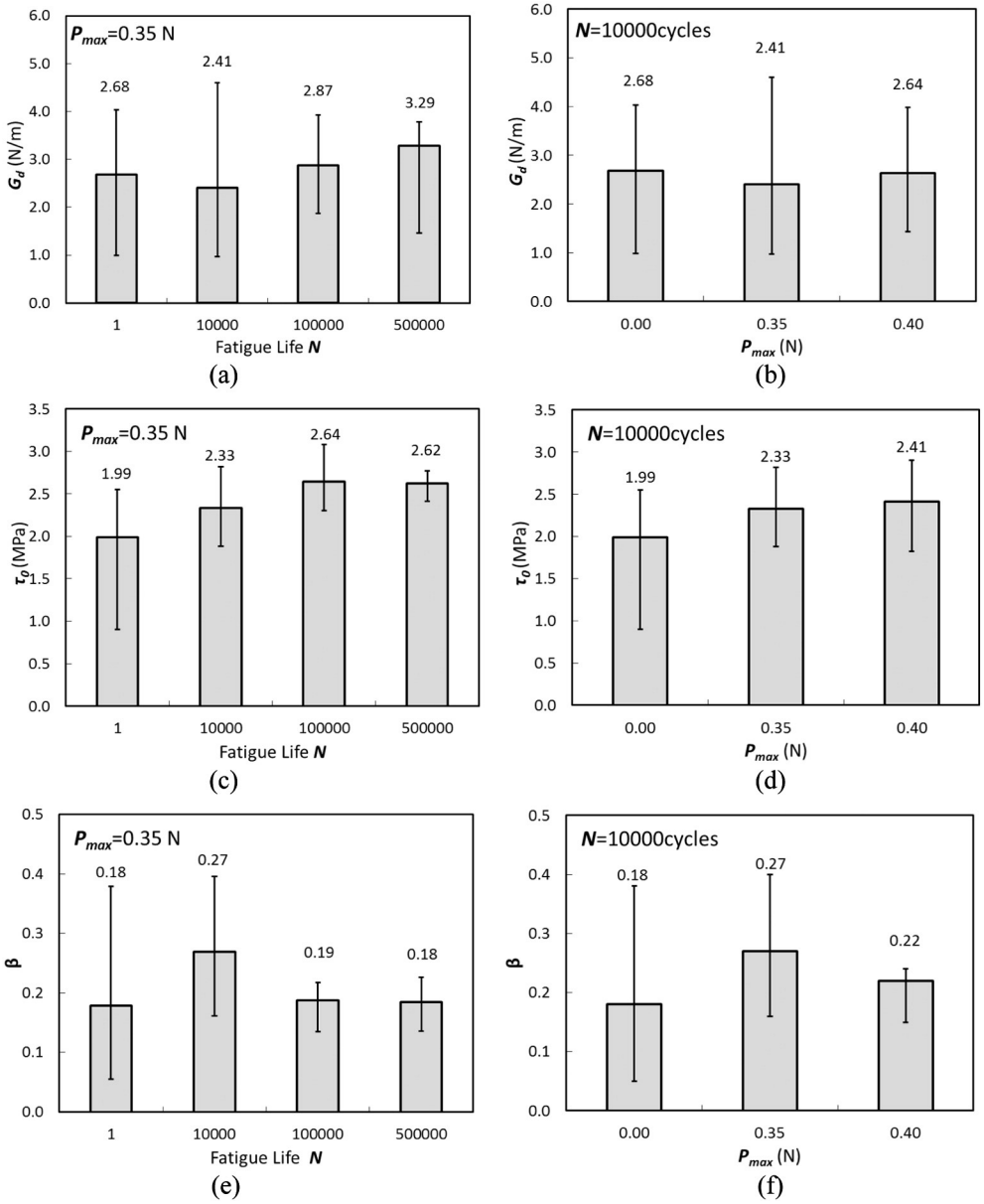


**Fig. 9.** Effects of fatigue cycle $N$ and fatigue loading level $P_{max}$ on chemical bond $G_d$ (a and b), frictional bond $\tau_0$ (c and d) and slip-hardening coefficient $\beta$ (e and f) subject to low-level fatigue.

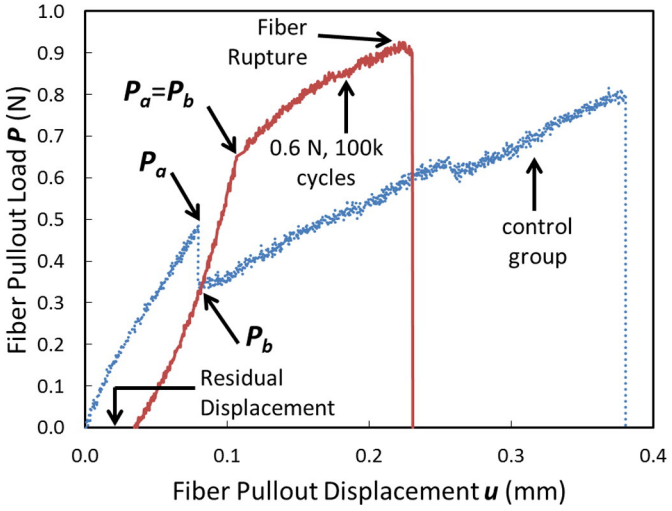


**Fig. 10.** Typical fiber pullout load-displacement ($P$-$u$) relation of control specimen and specimen that has experienced relatively high-level fatigue load ($P_{max} \geq 0.50$ N).

where $G_d$ and $\tau_0$ are the chemical bond and frictional bond, respectively, which can be determined from Eqs. (1) and (2) through the single fiber monotonic pullout test [22]; $\eta$ equals to $E_f V_f / E_m(1 - V_f)$, where $E_m$ is the Young's modulus of cement matrix and $V_f$ is fiber fraction by volume. Eq. (5) is derived from the fracture mechanics-based fiber debonding criterion and the force equilibrium when a fiber is being pulled out from matrix. Detailed derivation of Eq. (5) can be found in [30].

As can be seen in Fig. 5, fatigue-induced fiber debonding length $\Delta a$ increases with fatigue cycles $N$ as well as fatigue loading levels $P_{max}$. The fatigue-induced fiber debonding rate, i.e. the slope of the $\Delta a$-$N$ curve, as shown in Fig. 5b increases with the increase of load amplitude $P_{max} - P_{min}$, which can be described by a power function similar to the form of the Paris' Law [31] as Eq. (6).

$$\Delta a/N = C \cdot (P_{max} - P_{min})^M \tag{6}$$

where $C$ and $M$ are material related constants. Paris' Law was originally developed to capture crack propagation in bulk metallic materials under cyclic loads and to predict its fatigue life. Current study for the first time extends the concept of Paris' Law into a Type II fracture at the interface between flexible micro-fiber and hard cement matrix. It unveils the relation between the tunnel crack propagation rate and the fatigue amplitude of interfacial shear stress (or load) which enables prediction of fiber debonding in fiber composites subject to fatigue load.

### 3.1.2. Fatigue-induced fiber-matrix interface deterioration of debonding stage

At relatively low fatigue loading level, full debonding of fiber did not take place even at the end of the fatigue preloading. The effect of fatigue load on the fiber-matrix interface properties of the debonding stage is presented here. During the fatigue preloading phase, tensile stiffness of the single fiber pullout test was monitored and plotted as a function of fatigue cycles (Fig. 6). As can be seen, the stiffness increases with fatigue cycles up to about 10,000 cycles and remains steady afterwards. Since the tensile stiffness of the single fiber pullout test is governed by the tensile stiffness of the fiber and the fiber-matrix interface, tensile stiffness of fiber subject to fatigue was also measured by the single fiber fatigue test and plotted as a function of load cycles (Fig. 7). As can be seen, fiber stiffness continues to decrease with fatigue loads and therefore the increase of tensile stiffness of the single fiber pullout sample is attributed to changes of fiber-matrix interface properties during fatigue. At high fatigue cycle, fiber softens and mitigates continuous increase of tensile stiffness of the single fiber pullout sample as shown in Fig. 6.

To quantify fatigue-induced deterioration of fiber-matrix interface properties, monotonic reloading on the single fiber pullout specimen

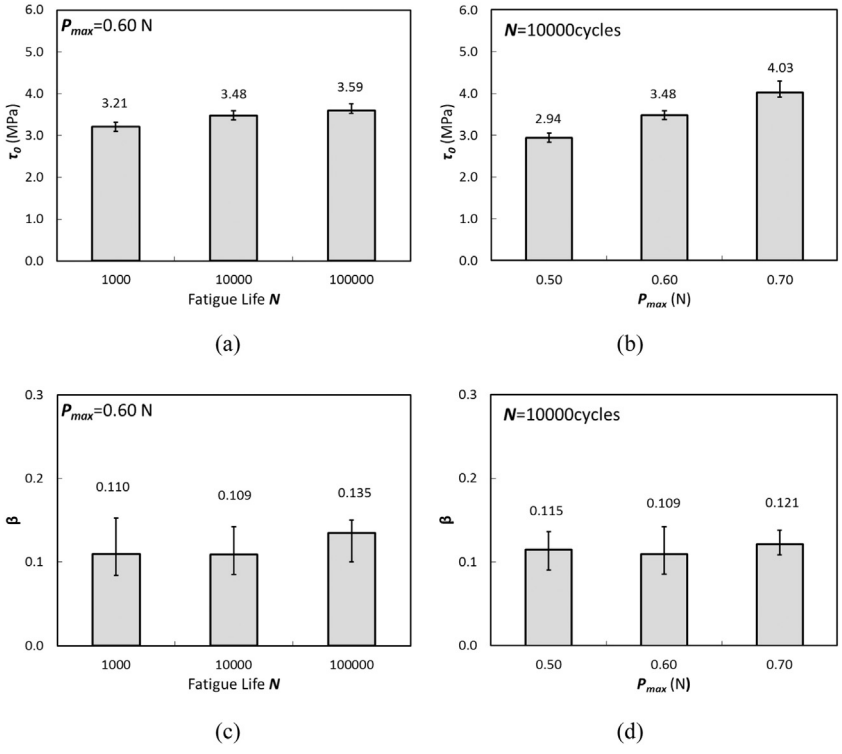


**Fig. 11.** Effects of fatigue cycle $N$ and fatigue loading level Pmax on frictional bond $\tau_0$ (a and b) and slip-hardening coefficient $\beta$ (c and d) subject to high-level fatigue.

was carried out after the fatigue preloading. Fig. 8 shows a typical single fiber pullout load versus fiber end displacement curve after low level fatigue preloading. The typical single fiber pullout curve of the control specimen, i.e. without fatigue preloading, was also plotted in the same figure. As can be seen, a sudden load drop from $P_a$ to $P_b$ can still be observed for samples with low level fatigue preloading. This is because the fiber was not completely debonded from the matrix during the fatigue preloading stage. In the debonding stage, the pullout load up to $P_a$ is resisted by the chemical adhesion $G_d$ of the undebonded interface, as well as the frictional bond $\tau_0$ of the debonded fiber-matrix interface. Upon full debonding, the pullout force $P_b$ is resisted by friction only [18]. $G_d$, $\tau_0$, and $\beta$ can therefore be determined based on the Eqs. (1) to (3) [18].

Fig. 9 plots fatigue-induced changes on interface properties at low level fatigue as functions of fatigue cycles $N$ and fatigue loading levels $P_{max}$. As can be seen, $G_d$ and $\beta$ are barely affected by fatigue loads while $\tau_0$ gets stronger with the increase of fatigue cycles as well as fatigue loading levels. The phenomenon of fatigue-induced friction enhancement at low level fatigue during fiber debonding stage is referred as *fatigue debonding hardening* in current study. This may be attributed to the damage of soft polymeric fiber caused by the reciprocated movement of debonded fiber portion against hard cement matrix subject to low level fatigue. A jamming effect can take place inside the matrix due to fiber or interface debris accumulation along the tunnel crack between the fiber-matrix interfaces. This leads to an increasing load resisting fiber pullout. Similar mechanisms have been suggested in soft fiber and hard matrix system subject to monotonic pullout force, which is referred as slip-hardening during fiber slippage stage after full debonding [28]. Such slip-hardening subject to monotonic pullout force was believed to be caused by damage of soft fiber and debris jamming during large sliding of fiber against hard matrix [18]. Current study reported for the first time such hardening can also occur during the fiber debonding stage when fiber-matrix interface is subject to low level fatigue. It is also noticed that there was residual displacement after the

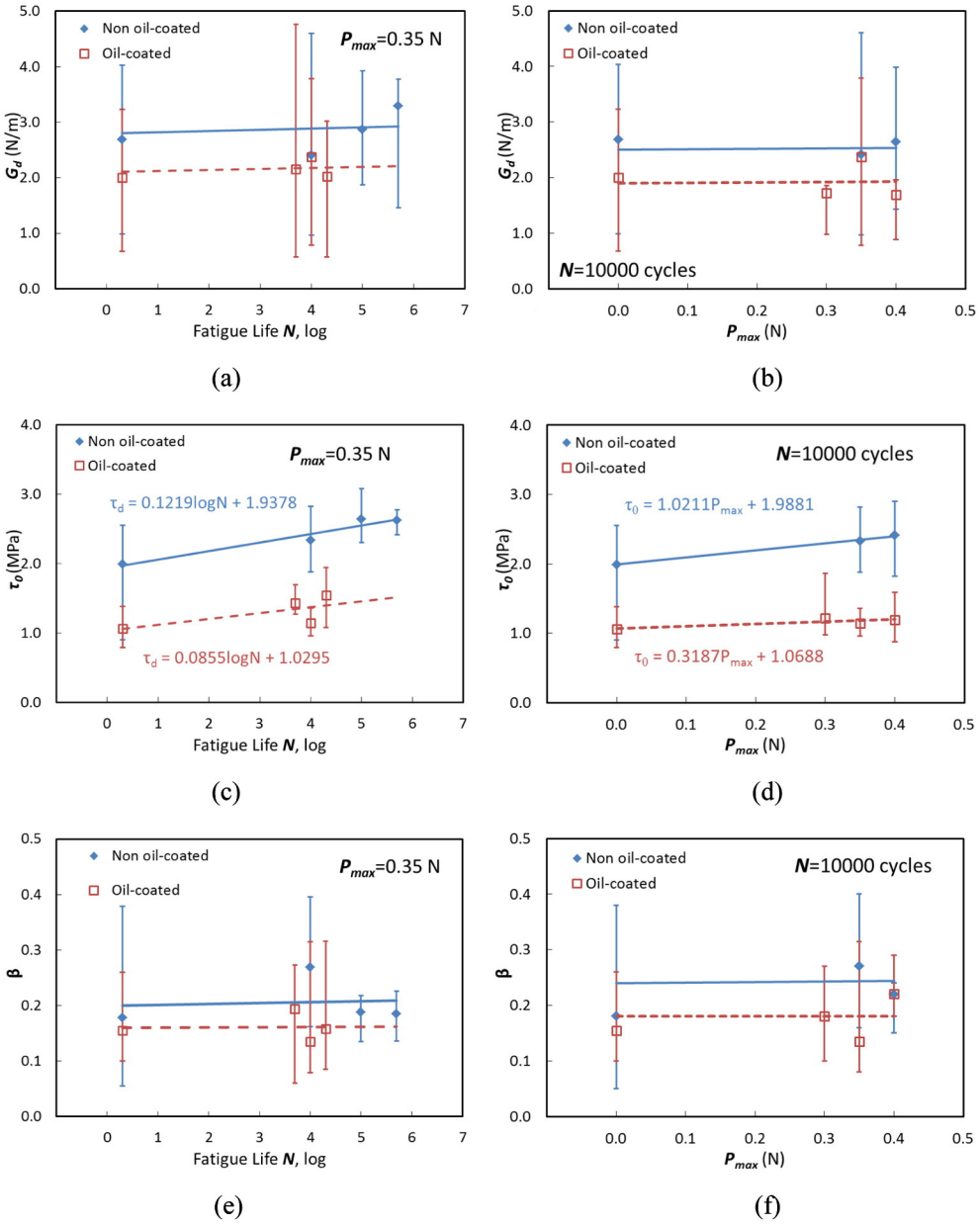


**Fig. 12.** Effect of fiber surface oil-treatment on the fatigue-induced interface deterioration of debonding stage: influence of fatigue cycle $N$ and fatigue loading level $P_{max}$ on chemical bond $G_d$ (a and b), frictional bond $\tau_0$ (c and d), and slip-hardening coefficient $\beta$ (e and f) for NOC and OC fibers.

fatigue preloading as shown in Fig. 8. This may be caused by the jamming of interface which prevent relaxation of fiber to its original position upon unloading.

*3.1.3. Fatigue-induced fiber-matrix interface deterioration of slippage stage*

At relatively high fatigue loading level, full debonding took place during the ramping phase of the fatigue preloading. The effect of fatigue load on the fiber-matrix interface properties of the slippage stage is presented here. Typical single fiber pullout load versus fiber end displacement after high level fatigue preloading is plotted together with that of the control specimen, i.e. without fatigue preloading, as Fig. 10. As the fiber is fully debonded during the ramping stage, the reloading pullout curve exhibits a bi-linear *P-u* behavior with no sudden load drop, i.e. $P_a = P_b$ and $G_d = 0$, which is distinct from the control specimen. As such, only $\tau_0$ and $\beta$ were calculated based on the Eqs. (2) and (3) [18].

Fig. 11 plots fatigue-induced changes on interface properties at high level fatigue as functions of fatigue cycles *N* and fatigue loading levels $P_{max}$. It can be seen that while $\tau_0$ is sensitive to fatigue load and increase with loading cycles *N* and loading level $P_{max}$, $\beta$ is not dependent on fatigue loads. The phenomenon of fatigue-induced $\tau_0$ enhancement at high level fatigue during fiber slippage stage is referred as *fatigue slippage hardening* in current study. This phenomenon may also be attributed to the jamming effect due to large reciprocated movement between debonded fiber and hard cement matrix subject to high level fatigue. The insensitivity of $\beta$ to both low and high fatigue loading levels indicates that slip-hardening effect is independent from the fatigue deterioration.

It should be noticed that both *fatigue debonding hardening* and *fatigue slippage hardening*, though increasing the friction between fiber and matrix, may be detrimental to some fiber composites where ductility and energy dissipation are required as increased interfacial bond can cause premature fiber rupture and prevents slippage of fibers. The following section will discuss using surface oil-treatment to mitigate such fatigue-induced hardening effects.

*3.2. Effect of fiber surface oil-treatment*

Surface oil-treatment of PVA fibers can effectively reduce fiber-matrix interfacial bond [28]. This section presents the influence of surface oil-treatment of PVA fiber on fatigue-induced deterioration of fiber-matrix interface. Fig. 12 compares the fatigue-induced fiber-matrix interface deteriorations of NOC and OC single fiber pullout specimens in the debonding stage. As can be seen, oil-treatment significantly weakens the interfacial bond properties $G_d$, $\tau_0$, and $\beta$. This can be attributed to that the oil mitigates the bond between the hydroxyl function group on the PVA fiber and the cementious matrix [28]. As described in the previous section, the chemical bond $G_d$ and slip-hardening coefficient $\beta$ of NOC specimens are not sensitive to fatigue load; as can be seen in Fig. 12, similar trend was observed for OC specimens. It again confirms the fatigue-independency of $G_d$ and $\beta$ when the loading level is low. But the frictional bond $\tau_0$ increases fatigue loads *N* and loading level $P_{max}$ for both NOC and OC specimens. As shown by the slope of linear trend lines, surface oil-treatment significantly mitigates the fatigue debonding hardening effect.

Fig. 13 compares the fatigue-induced fiber-matrix interface deteriorations of NOC and OC single fiber pullout specimens in the slippage stage. As debonding had been completed before reloading, $G_d$ equals to zero and therefore is not presented. It can be seen that oil-treatment significantly weakens the interfacial bond properties $\tau_0$ and $\beta$. Frictional bond $\tau_0$ continues to increase with fatigue loads *N* and loading level $P_{max}$, while the slip-hardening coefficient $\beta$ remains insensitive to fatigue loading. By comparing the slope of the linear trend lines, it is obvious that oil-treatment mitigates such fatigue slippage hardening effect.

The reduced fatigue-induced hardening effects could be attributed to the reduced interfacial bond by oil-treatment, which may mitigate fiber surface damage and the interface jamming at fiber-matrix during the reciprocated movement of the soft fiber and hard matrix. Fiber surface-oil treatment can be used as an effective technique to reduce the fatigue-induced fiber-matrix interface deterioration.

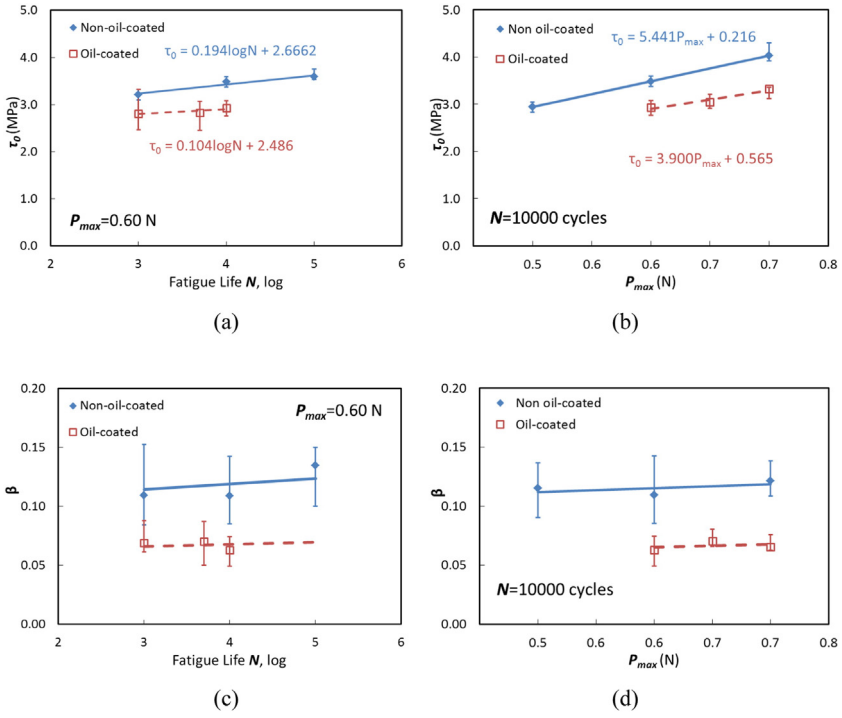


**Fig. 13.** Effect of fiber surface oil-treatment on the fatigue-induced interface deterioration of slippage stage: influence of fatigue cycle *N* and fatigue loading level $P_{max}$ on frictional bond $\tau_0$ (a and b) and slip-hardening coefficient $\beta$ (c and d) for NOC and OC fibers.

## 4. Conclusions

This study experimentally investigated the deterioration mechanism of flexible fibers in brittle matrix subject to fatigue load. Specifically, the effect of fatigue-induced deterioration of interface between micro-PVA fiber and cement matrix was studied through the single fiber fatigue pullout test and the micro-structural deterioration mechanism of the fiber-matrix interface under fatigue load was unveiled.

It was found that fatigue load is able to propagate the tunnel crack along the fiber-matrix interface, i.e. *fatigue-induced fiber debonding*, and an empirical relation between debonding rate and fatigue loading level similar to the Paris' law was suggested. It was observed that interface chemical bond $G_d$ and the slip-hardening coefficient $\beta$ were fatigue independent while $\tau_0$ increased with fatigue cycles $N$ and fatigue loading levels $P_{max}$. Such fatigue-induced interface hardening can occur during fiber debonding stage, i.e. *fatigue debonding hardening*, as well as during fiber slippage stage, i.e. *fatigue slippage hardening*. Oil-treatment on surface of PVA fiber was demonstrated as a mean to mitigate such fatigue-induced interface hardening.

## Acknowledgement

The authors would like to acknowledge financial supports from the SinBerBEST program, National Research Foundation Singapore [NRFCRP8-2011-03] and from Nanyang Technological University, Singapore (COE_SUG/RSS_19MAR10_1/23).

## References

[1] J. Bai, Advanced Fibre-reinforced Polymer (FRP) Composites for Structural Applications, Elsevier, 2013.
[2] C. Bakis, L.C. Bank, V. Brown, E. Cosenza, J. Davalos, J. Lesko, A. Machida, S. Rizkalla, T. Triantafillou, Fiber-reinforced polymer composites for construction-state-of-the-art review, J. Compos. Constr. 6 (2002) 73–87.
[3] C. Yang, S. Jeng, J.-M. Yang, Interfacial properties measurement for SiC fiber-reinforced titanium alloy composites, Scr. Metall. Mater. 24 (1990) 469–474.
[4] S. Senet, R. Grimes, D. Hunn, K. White, Elevated temperature fracture behavior of a 2-D discontinuous fiber reinforced carbon/carbon composite, Carbon 29 (1991) 1039–1049.
[5] A.M. Brandt, Fibre reinforced cement-based (FRC) composites after over 40 years of development in building and civil engineering, Compos. Struct. 86 (2008) 3–9.
[6] F. de Andrade Silva, B. Mobasher, R.D. Toledo Filho, Cracking mechanisms in durable sisal fiber reinforced cement composites, Cem. Concr. Compos. 31 (2009) 721–730.
[7] M. Sun, Q. Liu, Z. Li, Y. Hu, A study of piezoelectric properties of carbon fiber reinforced concrete and plain cement paste during dynamic loading, Cem. Concr. Res. 30 (2000) 1593–1595.
[8] P. Song, S. Hwang, Mechanical properties of high-strength steel fiber-reinforced concrete, Constr. Build. Mater. 18 (2004) 669–673.
[9] P. Song, S. Hwang, B. Sheu, Strength properties of nylon-and polypropylene-fiber-reinforced concretes, Cem. Concr. Res. 35 (2005) 1546–1550.
[10] V.C. Li, S. Wang, C. Wu, Tensile strain-hardening behavior of polyvinyl alcohol engineered cementitious composite (PVA-ECC), ACI Mater. J. 98 (2001) 483–492.
[11] Y. Yang, M.D. Lepech, E.-H. Yang, V.C. Li, Autogenous healing of engineered cementitious composites under wet–dry cycles, Cem. Concr. Res. 39 (2009) 382–390.
[12] M. Şahmaran, V.C. Li, Influence of microcracking on water absorption and sorptivity of ECC, Mater. Struct. 42 (2009) 593–603.
[13] Z. Bayasi, M. Al Dhaheri, Effect of exposure to elevated temperature on polypropylene fiber-reinforced concrete, ACI Mater. J. 99 (2002) 22–26.
[14] S. Wen, D. Chung, Self-sensing of flexural damage and strain in carbon fiber reinforced cement and effect of embedded steel reinforcing bars, Carbon 44 (2006) 1496–1502.
[15] A. Katz, V.C. Li, A. Kazmer, Bond properties of carbon fibers in cementitious matrix, J. Mater. Civ. Eng. 7 (1995) 125–128.
[16] A.E. Naaman, H. Najm, Bond-slip mechanisms of steel fibers in concrete, ACI Mater. J. 88 (1991) 135–145.
[17] T. Kanda, V.C. Li, Interface property and apparent strength of high-strength hydrophilic fiber in cement matrix, J. Mater. Civ. Eng. 10 (1998) 5–13.
[18] C. Redon, V.C. Li, C. Wu, H. Hoshiro, T. Saito, A. Ogawa, Measuring and modifying interface properties of PVA fibers in ECC matrix, J. Mater. Civ. Eng. 13 (2001) 399–406.
[19] W. Wang, S. Wu, H. Dai, Fatigue behavior and life prediction of carbon fiber reinforced concrete under cyclic flexural loading, Mater. Sci. Eng. A 434 (2006) 347–351.
[20] S. Wei, G. Jianming, Y. Yun, Study of the fatigue performance and damage mechanism of steel fiber reinforced concrete, ACI Mater. J. 93 (1996) 206–212.
[21] Z. Jun, H. Stang, Fatigue performance in flexure of fiber reinforced concrete, ACI Mater. J. 95 (1998) 58–67.
[22] P. Jun, V. Mechtcherine, Behaviour of strain-hardening cement-based composites (SHCC) under monotonic and cyclic tensile loading: part 1-experimental investigations, Cem. Concr. Compos. 32 (2010) 801–809.
[23] P. Jun, V. Mechtcherine, Behaviour of strain-hardening cement-based composites (SHCC) under monotonic and cyclic tensile loading: part 2-modeling, Cem. Concr. Compos. 32 (2010) 810–818.
[24] S. Muller, V. Mechtcherine, M. Zydek, Behaviour of strain-hardening cement-based composites (SHCC) subject to cyclic loading, in: H.W. Reinhardt (Ed.), 7th International RILEM Workshop on High Performance Fiber Reinforced Cement Composites (HPFRCC), Stutggart, Germany, 2015.
[25] S. Qian, Influence of Concrete Material Ductility on the Behavior of High Stress Concentration Zones(PhD Thesis) University of Michigan, 2007.
[26] P. Suthiwarapirak, T. Matsumoto, T. Kanda, Multiple cracking and fiber bridging characteristics of engineered cementitious composites under fatigue flexure, J. Mater. Civ. Eng. 16 (2004) 433–443.
[27] J. Qiu, E.-H. Yang, Study on fatigue failure of polymeric fiber-reinforced strain-hardening cementitious composites, in: E. Schlangen (Ed.), 3rd International RELIM Conference on Strain Hardening Cementitious Composites, Netherlands, Dordrecht, 2014.
[28] V.C. Li, C. Wu, S. Wang, A. Ogawa, T. Saito, Interface tailoring for strain-hardening polyvinyl alcohol-engineered cementitious composite (PVA-ECC), ACI Mater. J. 99 (2002) 463–472.
[29] A. Katz, V.C. Li, A special technique for determining the bond strength of micro-fibres in cement matrix by pullout test, J. Mater. Sci. Lett. 15 (1996) 1821–1823.
[30] Z. Lin, T. Kanda, V.C. Li, On interface property characterization and performance of fiber reinforced cementitious composites, Concr. Sci. Eng. 1 (1999) 173–184.
[31] L. Pook, N. Frost, A fatigue crack growth theory, Int. J. Fract. 9 (1973) 53–61.